

RESISTIVITY AND PERMEABILITY MAPPING AT THE LAMINA SCALE

M.A. Jackson, D.G. Bowen, J.L. Jensen and A.C. Todd
Heriot-Watt University

Abstract

The physics of transport through porous media indicates that there should be an underlying functional relationship between permeability and resistivity. Despite this, previously published experiments have usually failed to demonstrate a convincing relationship. We think this is because the volumes of rock investigated included unaccounted for geological heterogeneities.

We explored the relationship between resistivity and permeability in sedimentary rocks at the sub-lamina scale, using a probe permeameter and a new resistivity probe for the measurements. The resistivity probe has a functional geometry comparable to existing probe permeameter instruments.

Measurements were made on a highly laminated aeolian sandstone sample. When compared, maps of both resistivity and permeability showed a similar character. We noted a strong correlation between conductivity and permeability. The resistivity data could be used to predict the probe permeability to, at worst, within $\pm 40\%$ (one standard deviation).

These results provide evidence that permeability within individual laminae may be accurately predicted from resistivity data, *when acquired at similar scales*. Development of a method for obtaining reliable resistivity - permeability relationships would improve assessment of the rock flow characteristics using wireline micro-resistivity data.

Introduction

The absolute value of permeability and its degree of variability over various scales are key parameters in effective reservoir description and management. For example, large scale (10's of meters) permeability variations such as those inherent in faults or shales can lead to compartmentalisation and entrapment of hydrocarbons. Small scale (mm-cm) permeability variations impact on the level of competition between viscous and capillary forces and the efficiency of oil displacement (Ringrose et al., 1993).

Existing probe permeameters enable routine measurement of rock permeability at the small scale (Lewis et al., 1990; Brendsdal and Halvorsen, 1992). Dense permeability data sets can be gathered using automated instruments (e.g., Jones, 1992) and such data sets have been used to estimate recovery performance in laminated sandstones (Corbett and Jensen, 1993). The usefulness of core data sets, however, depends upon good recovery and careful sample preparation.

Detailed probe permeameter data sets could be augmented by appropriate resistivity measurements. Flow models could then be developed from small scale permeability estimates derived from wireline resistivity imaging tools (Ekstrom et al., 1987; Bourke, 1993). Such a procedure, however, would be possible only if an appropriate relationship between rock resistivity and permeability could be established.

This paper describes how a small scale permeability--resistivity relationship can be obtained. We suggest why past attempts at exploiting the resistivity--permeability relation may have been disappointing and how, by carefully accounting for small scale variability, we obtain more robust results. The practical design of a resistivity probe,

comparable in investigative geometry to the probe permeameter, is also presented, together with the results obtained. The effects of surface electrokinetics are not directly addressed in the following analysis (Sherman 1988); the experimental parameters were deliberately chosen to minimise interference from these effects.

Theory

The existence of a simple relationship between resistivity (ρ) and permeability (k) has been recognised for decades. Muskat (1937) pointed out, for example, that the equations governing macroscopic steady state, incompressible fluid flow and electrical current flow are identical: Voltage (V) is analogous to pressure (p), conductivity ($\sigma=\rho^{-1}$) is analogous to mobility (k/μ), and Ohm's law is analogous to Darcy's law. If a system matrix is non-conductive for both electric current and fluid flow, then the flow paths are similar. This is not the case for most other forms of energy, where the matrix would conduct an appreciable portion of the energy. Therefore one analogue could be used to predict the behaviour of the other. Muskat (1937) exploited the electrical analogue to solve otherwise intractable large scale reservoir engineering problems.

The analogy between current and fluid flow, however, is not perfect. Muskat (1937) pointed out that the current-fluid flow analogue only applies where the permeability may be assumed to be homogeneous and isotropic. At the pore scale this assumption breaks down. In a non-conductive matrix, the electrical and fluid conductivities respond differently to the pore geometries; fluid flow encounters viscous drag while current flow does not. For example, in the simple case of a capillary tube of radius r , the electrical conductance is proportional to r^2 while the hydraulic conductance is proportional to r^4 (e.g., Matheron, 1967; Doyen, 1988).

A physical requirement for homogeneity and isotropy implies that one lamination is the largest geological element which should be considered in order to get the best from the fluid-current analogue. Even rocks which to the naked eye appear to have no lamination may be laminated and have an order of magnitude variation in permeability (Brendsdal and Halvorsen, 1992). More strongly laminated materials may have two or three orders of magnitude of permeability variation between laminations (Brendsdal and Halvorsen, 1992). Clearly, the fluid-current flow analogue will work best when the volume of interest lies between the pore and the lamination scales.

Many investigators have examined the permeability-resistivity relationship at scales outside this range. Perhaps Archie's (1942, 1950) study is best known. He correlated F with ϕ and k of core plugs in the ranges of 15-40% ϕ . However, in his Miocene Gulf Coast sandstone example, the F - ϕ relationship appears considerably weaker than the F - k relation. Also, in the Nacatoch Formation (Fig. 1), the F - ϕ plot has a much larger range of F values (5 to 100) than the F - k plot (5 to 30). Values of $k < 0.1$ mD were not recorded, making the F - ϕ relationship appear more convincing. Thus, even from Archie's own evidence, it is generally difficult to judge whether the F - k relationship is better or worse than the F - ϕ relationship. Similar studies (e.g., Mazác et al., 1985; Gorman and Kelly, 1990) have also shown mixed behaviour to support either relationship and, to our knowledge, all have been conducted on samples at a scale larger than the lamination level.

In an attempt to identify the fundamental F - k relationships, there have been a number of studies modelling conductivity at the pore scale. The bundled capillary tube model was perhaps the first. It implies, however, that the entire pore system contributes to formation conductance (both hydraulic and electric). In observations of electrical

conductance as a function of the pore volume occupied by intruding mercury (Katz and Thompson, 1987), typically just 25% of the pore space contributes to over 80% of a rock's electrical conductivity. Herrick and Kennedy (1993) report a similar behaviour. According to percolation theory models (e.g., Ambegaokar et al., 1971), the overall resistance to transport in pore networks is controlled by elements with a conductance greater than a threshold value. By considering the probability of a given pore forming part of an interconnected network (and hence contributing to electric current conductivity), a model rock conductivity value can be calculated. At the large end of the pore size distribution, there are a few very large pores. Although they are responsible for localised high conductivity zones, by virtue of their infrequent occurrence, they are less likely to be laterally extensive. Consequently they contribute little to the overall conductivity. Small pores are less conductive and likewise do not greatly contribute to overall conductivity. This leads to the concept of a characteristic length, l_c , which defines an effective pore dimension that maximises the electrical conductance function. Based on the characteristic length and the proportion of the pore space contributing to conductivity, Katz and Thompson (1987) derived a model for rock conductivity in terms of parameters derived from mercury injection experiments. They found that $\sigma \propto l_c$ and $k \propto l_c^3$. Doyen (1988) obtained similar expressions. While these models describe the relationship between pore network geometry and electrical resistivity of a rock in physically realistic manners, their field application is limited as it is expressed in terms of fixed physical parameters that can currently only be obtained for a particular rock by destructive laboratory experiments. Nonetheless, these results explain why, at the macroscopic scale, permeability typically varies by three orders of magnitude while conductivity only varies by one (Fig. 1).

In summary, the resistivity-permeability relationship can be expected to apply best over a small range of scales. At the pore scale (10's-100's μm), various studies have shown that current and fluid flows respond to the pore geometries differently. At the lamina set scale (cm's), permeability heterogeneity within the samples may diminish the relationship. Thus, the most appropriate scale to observe and exploit the current-fluid flow relationship is at the lamination scale (mm-cm). We now describe a resistivity probe having a volume of investigation similar to the probe permeameter and some experimental results.

Resistivity Probe Design

To be able to directly compare resistivity and permeability data from a heterogeneous laminated rock, it is essential that both sets of measurements respond to identical rock volumes. A commercial pressure decay probe permeameter (Jones, 1992) was used to measure permeability over grid-points on the face of a rock slab. The dimensions of the probe permeameter probe tip and sealing assembly determine both the measurement geometric constant (G_0) and the volume of investigation (Goggin et al, 1988).

Probe resistivity measurements were recorded that were representative of nearly identical rock volumes to the probe permeameter data. This was achieved by constructing a resistivity device having a probe electrode of equal diameter to the inside diameter of the probe permeameter probe tip and a sealing insulator arrangement with similar dimensions to the probe tip seal. Equivalent far-field (boundary) conditions were established by immersing the entire rock sample in a conductive brine. A ground (zero potential) electrode of sufficiently large area was used to ensure that the measurement current flow did not cause a localised increase in ground potential. To meet these requirements, a flat lead electrode was placed across the bottom of a glass tray and the rock sample was submerged to a depth greater than the depth of investigation of the measurement. To provide mechanical support, a perforated non-conductive spacer (Fig. 2) was used to stand the sample off the bottom by approximately 8 mm.

The probe (Fig. 3) incorporated a simple tip-seal design consisting of an insulating body containing a sprung electrode surmounted by a single 'O'-ring. As the probe is lowered, the electrode is compressed against its spring until the 'O'-ring first seals against the rock. Then, with further compression, brine is excluded from between the insulator body and the probe tip, thereby forcing the current to pass from the tip electrode through the rock sample and around the insulator to the return (zero potential) electrode. The permeameter probe tip is constructed so as to minimise the tendency of the seal tip to deform as the application pressure is increased. While measuring, a head-space of approximately 2 mm is maintained between the probe body and the sample surface. This space is sufficient to ensure the probe body itself does not present any restriction to the flow of the measuring gas as it permeates the sample surface. However, for the resistivity probe, the contrast in conductivity between the measured sample and the surrounding zero potential is considerably less than that for permeability. To ensure that the geometric factor is not affected by the probe body, the electrical insulator near the tip seal must have the same outer diameter as the tip seal along a length comparable with the depth of investigation. This constraint prevents mechanical containment of the tip seal 'O'-ring as is done in probe permeameter probe tips. As a consequence, the resistivity probe geometric factor is expected to show more sensitivity to the application force.

Conversion of Apparent Resistance to Formation Resistivity

The probe permeameter equation (Goggin et al., 1988) relating injection (p_1) and ambient (p_0) gas pressures, gas viscosity (μ), flow rate (q), and tip inner radius (r_i) to apparent permeability (k_{app}) is:

$$k_{app} = \frac{q\mu p_1}{G_0^k r_i \frac{p_1^2 - p_0^2}{2}}, \quad (1)$$

where G_0^k is the geometric factor for the probe tip. G_0^k contains information concerning the seal and sample geometries. In an analogous manner, apparent resistivity, ρ_{app} , is calculated from apparent resistance using the equation

$$\frac{1}{\rho_{app}} = \sigma = \frac{1}{G_0^r r_i R_{app}} \quad (2)$$

where G_0^r is the geometric factor for the resistivity tip. This was established from the steady-state half-space solution presented by Goggin et al (1988). The formation factor, F , is calculated from

$$F = \frac{\rho_{app}}{\rho_w}, \quad (3)$$

and is the apparent resistivity normalised to the pore fluid resistivity (ρ_w). The $G_0^r r_i$ for the experimental resistivity probe was 0.01145 cm. This is very close to the value for the permeameter probe. Experimental verification of the probe geometric factor will require the fabrication of an impermeable resistivity standard from a material such as doped silicon.

Experimental Setup

A slab of a commercially quarried aeolian New Red Sandstone of Permian age (Greig, 1971) was cut so as to display laminations approximately parallel to the slab sides. Locharbriggs Sandstone exhibits distinct parallel laminations characteristic of aeolian

stoss slope grain flow deposition (Ahlbrandt and Fryberger, 1981). Grain size varied from medium to fine across the sample. The grains were rounded to sub-rounded and moderately to well sorted within individual laminae. The rock possessed obvious visual heterogeneities at the lamina scale. The heterogeneity enabled measurements to be taken over a sufficient range of values so that a significant correlation between resistivity and permeability could be examined within the one sample.

Probe permeameter measurements were made using a probe tip having an inner tip seal radius (r_i) of 2.29 mm and a dimensionless tip seal thickness (b_0) of 2.017, which, for the half-space boundary conditions of this experiment, results in a ($G_0^k r_i$) of 0.0116 cm. A 2 mm grid of measurements was recorded over one slab face, and the results displayed in the form of a grey-scale image (Fig. 4). Measured permeabilities were in the range 56 to 3900 millidarcies.

The rock slab was evacuated then pressure saturated with brine prior to making the resistivity measurements. As a compromise between minimising surface electrokinetic effects and ease of handling, a 100,000 mg/l NaCl brine was selected as the saturating medium. Once saturated, the slab remained immersed in the brine throughout the experimental stage.

A manually operated steady-state permeameter was adapted for making resistivity measurements (Fig 5). The probe was mounted on an adjustable height table and controlled by a pneumatic cylinder, capable of raising and lowering it onto the sample with a repeatable force. Linear displacement indicators allowed accurate manual placement of the probe relative to a known point on the sample.

A precision digital component analyser was used to make measurements of both impedance and phase shift at three frequencies (1, 10, 100 kHz). Good probe contact was ensured by maintaining the 1 kHz phase shift at a value less than 3 degrees for each measuring point. By plotting impedance against measurement frequency, it was determined that less than 0.1% correction was required to extrapolate the 1kHz measurements to an equivalent DC resistance. Hence, the 1kHz impedance was considered the equivalent to DC resistance.

Since the system had to achieve stability at each measuring point, data acquisition covered a period of several days. This work comprised a scoping study of the feasibility of the probe resistivity measurements and a requirement for inert electrodes was deliberately not specified. Hence, despite sealing the measurement cell between measurement runs, some chemical reactions between the saturating brine, the air, the sample and the electrodes occurred. Data recorded subsequent to the initial few days work with the fresh brine were adversely affected and, in the interests of accuracy and brevity, only a limited portion of the slab was scanned for resistivity.

Experimental Results

Resistivity data recorded over the upper section of the slab were displayed in a grey-scale image (Fig. 6). The data were inverted prior to display to better the match the permeability map (Fig. 5). High conductivity (permeability) areas are dark and low conductivity (permeability) regions are light. The resistivity and permeability images clearly show the low permeability lamination near the top of the slab.

A good straight line fit was obtained on a log-log plot of F versus k (Fig. 7). The regression line shown ($R^2 = 0.90$) has the equation:

$$\ln(k_{est}) = 20.9 - 5.77 \cdot \ln(F) \quad (4)$$

with the estimated permeability (k_{est}) in millidarcies. The standard errors for the coefficients in Equation (4) are 20.9 ± 0.21 and 5.77 ± 0.08 . Equation (4) gives the predictor

$$k_{est} = 1.29 \times 10^9 \times F^{5.8} \quad (5)$$

where a correction for bias has been included in the detransformation (Jensen and Lake, 1985). The greater data scatter seen at high values (Fig. 6) is in part a consequence of small-scale heterogeneity. Microscopic studies of Locharbriggs sandstone have revealed localised clusters of extremely coarse pores. The dimensions of these high conductivity features can be large enough to violate the assumptions of homogeneity and isotropy that apply to the $G_0^f r_i$ of the probes used.

Discussion

The strong experimental correlation obtained for the Locharbriggs sandstone sample tested indicates that there is an underlying physical relationship between electrical resistivity and permeability. Matheron's (1967) arguments, based at the pore level, that there will only be a weak and distant macroscopic relationship between electrical and hydraulic properties are not supported by the data. He is, however, correct to claim that F and k will not vary by the same amount because of the different sensitivities of the two processes to the pore geometry. We have tested the relationship at the scale where the pore size distribution within a sample volume is least variable (homogeneous, isotropic permeability) but encompasses numerous pores.

For pore systems that exhibit significant variability in their pore size distributions at the small-scale, e.g. the bimodal distributions of Diederix et al (1982), we would expect both Archie-like behaviour and k - F relationships to break down. We expect that different F - k relationships would need to be determined for different facies and that the relationship would be weaker for poorly sorted materials. Diagenetic effects could also cause the relationship to weaken.

The reader may conclude that, since there is a non-trivial dependence on characterising the pore system geometry, there is little prospect for establishing a robust relationship between permeability and electrical resistivity. However, by considering other than direct current electrical conductivity, there may be a means to differentiate the portion of the total pore structure that contributes to a rock's permeability and electrical conductivity. For direct current resistivity, only the physically interconnected pore space contributes to conductivity (surface effects neglected). At higher frequencies, capacitive coupling between adjacent non-directly connected pores contributes to the quadrature (imaginary) component of a rock's impedance (Sherman, 1988). If a relationship between connected and non-interconnected pore space can be established using high frequency measurements, a method of characterising l_c , and hence permeability from down hole measurements may follow.

Conclusions

- Historically, empirical correlations have been used to predict permeability from porosity and resistivity measurements. By examining the physics of transport in porous media, a direct functional relationship can be argued between rock conductivity and permeability which avoids reliance on empirical relations linked through porosity. The physical basis for the observed shortcomings in commonly applied correlations can be explained in terms of heterogeneity within the volumes sampled.

- Lamina scale heterogeneities may be responsible for the apparent weakness of the correlations of resistivity and permeability that form the basis of current resistivity log interpretation techniques. A stronger correlation can be obtained by comparing measurements made at an appropriate scale so as to minimise the perturbing effects of heterogeneities. Scaleup of these data can be achieved through the Geopseudo approach (Ringrose et al, 1993)
- A practical resistivity measuring device having a comparable geometry of measurement to existing probe permeameter instruments has been designed, built and tested, thereby demonstrating the feasibility of the probe resistivity measurement method.
- Mapping of both probe permeameter and resistivity measurements shows they correlate well and with visually observable textural features in a well sorted, aeolian sample. A crossplot of small-scale resistivity and permeameter data identified a strong correlation ($R^2 = 0.90$) between formation factor and permeability.
- Within a given sedimentary unit, permeability can be expressed as an exponential function of brine saturated rock resistivity. The theoretical basis for this relationship dictates that the exponent is related to a particular sediment type as reflected in the geometric arrangement of the pore structure, and may not be generally applicable to other sedimentary units.
- At present, the complexity of actual rock pore systems defies accurate characterisation except using methods such as destructive mercury injection experiments or empirical correlations. Understanding of the pore system geometry and behaviour resulting from mercury injection experiments may result in the development of useful relationships between measurable down hole parameters and rock permeability.

Nomenclature

b_D	dimensionless tip seal radius (ratio of outer to inner radius)
F	formation factor
G_0	geometric factor
G_0^k	geometric factor for permeameter tip
G_0^r	geometric factor for resistivity tip
k	permeability (mD)
l_c	characteristic pore size (μm)
m	cementation exponent
p	pressure (bar)
q	flow rate (cc/sec)
r	radius of capillary (μm) or tip (mm)
V	electric potential (Volts)
ϕ	porosity (fraction occupied by the saturating medium)
ρ	electrical resistivity (ohm-metres)
σ	electrical conductivity (sm^{-1})
μ	fluid viscosity (cp)

Acknowledgements

The work described in this paper was carried out in the Department of Petroleum Engineering, Heriot-Watt University, Edinburgh, Scotland, in partial fulfilment of the requirements of the Degree of Master of Engineering. The support and assistance of the workshop staff is gratefully acknowledged.

References

- Ahlbrandt, T.S., & Fryberger, S.G., 1981. Introduction to Eolian Deposits, in Sandstone Depositional Environments, Am. Assoc. Pet Geol., Tulsa.
- Ambegaokar, V., Halperin, & B.I., Langer, J.S. 1971. Hopping Conductivity in Disordered Systems, Phys. Rev. B, **4**, 2612 - 2620.
- Archie, G. E., 1950. Introduction to Petrophysics of reservoir rocks, AAPG Bul. **34**, pp. 943-961
- Archie, G.E., 1942. The Electrical Resistivity Log as an Aid in Determining Some Reservoir Characteristics, SPE - AIME Transactions, **146**, pp. 54 - 62.
- Bourke, L. T., 1993. Core Permeametry Imaging: Its Relevance to Conventional Core Characterisation and Potential Applications to Wireline Measurement, Marine and Petroleum Geology., **10**, 318-324.
- Brendsdal, A., & Halvorsen, C., 1992. Quantification of Permeability Variations Across Thin Laminae in Cross Bedded Sandstone, in Advances in Core Evaluation III: Reservoir Management ed. by P. F. Worthington & C. Chardaire-Rivière, Gordon and Breach Science Publishers, Paris, 25-42.
- Corbett, P. W. M., & Jensen, J. L., 1993. An Application of Probe Permeametry to Prediction of Two-Phase Flow Performance in Laminated Sandstones (Lower Brent Group, North Sea), Marine & Petroleum Geology., **10**, 335-346.
- Diederix, K.M., 1982. Anomalous Relationships Between Resistivity Index & Water Saturations in the Rotliegend Sandstone (The Netherlands), Transactions of the SPWLA 23rd Annual Logging Symposium.
- Doyen, P. M., 1988. Permeability, Conductivity, and Pore Geometry of Sandstone, J. Geophysical Res., **93**, 7729-7740.
- Ekstrom, M.P., Dahan, C.A., Chen, M.Y., Lloyd, P.M., & Rossi, D.J., 1987. Formation Imaging with Microelectrical Scanning Arrays, The Log Analyst, **28**, 294 - 306.
- Goggin, D.J., Thrasher, R.L. & Lake, L.W., 1988. A Theoretical and Experimental Analysis of Mini-permeameter Response Including Gas Slippage and High Velocity Flow Effects, In Situ, **12**, 79-116.
- Gorman, T., & Kelley, W. E., 1990. Electrical-Hydraulic Properties of Unsaturated Ottawa Sands, J. Hydrol., **118**, 1-18.
- Greig, D.C., 1971. British Regional Geology - The South of Scotland, HMSO.
- Herrick, D.C. & Kennedy, W.D., Electrical Efficiency: A Pore Geometric Model For The Electrical Properties Of Rocks, SPWLA Paper HH, 34th Ann. Log. Symp., Calgary, Alberta, June 13-16 1993.
- Jensen, J. L., & Lake, L. W., 1985. Optimisation of Regression-Based Porosity-Permeability Predictions, Transactions paper R of The Tenth Formation Evaluation Symposium CWLS Calgary, Sept. 29-Oct. 2.
- Jones, S.C., 1992. The Profile Permeameter - A New, Fast, Accurate Minipermeameter, SPE 24757 - 67th Annual SPE Conference. Oct 4-7, Washington DC.
- Katz, A.J., & Thompson, A.H., 1987. Prediction of Rock Electrical Conductivity From Mercury Injection Measurements, J. Geophysical Research, **92**, 599-607.
- Lewis, J.J.M., Lowden, B., & Hurst, A., 1990. Permeability Distribution and Measurement of Reservoir Scale Heterogeneities in the Lochaline Sandstone (Cretaceous) , Field Guide, 13th Int'l Sedimentological Conference, August.
- Lovell, M.A., & Jackson, P.D., 1991. Electrical Flow in Rocks: The Application of Resolution Electrical Resistivity Core Measurements, SPWLA 32nd Annual Logging Symposium, Paper H.
- Matheron, G., 1967. Éléments Pour une Théorie des Milieux Poreux, Masson, Paris.
- Mazác, O., Kelley, W. E., & Landa, I., 1985. A Hydrogeophysical Model for Relations Between Electrical & Hydraulic Properties of Aquifers, J. Hydrol., **79**, 1-19.
- Muskat, M., 1937. The Flow of Homogeneous Fluids Through Porous Media, McGraw-Hill Book Co., New York.
- Ringrose, P.S., Sorbie, K.S., Corbett, P.W.M., & Jensen, J.L., 1993. Immiscible Flow Behaviour in Laminated & Crossbedded Sandstones , J. Petroleum Science & Engineering, **9**, 103 - 124.
- Sherman, M.M., 1988. A Model for the Frequency Dependence of the Dielectric Permittivity of Reservoir Rocks, The Log Analyst, **29**, 358 - 369

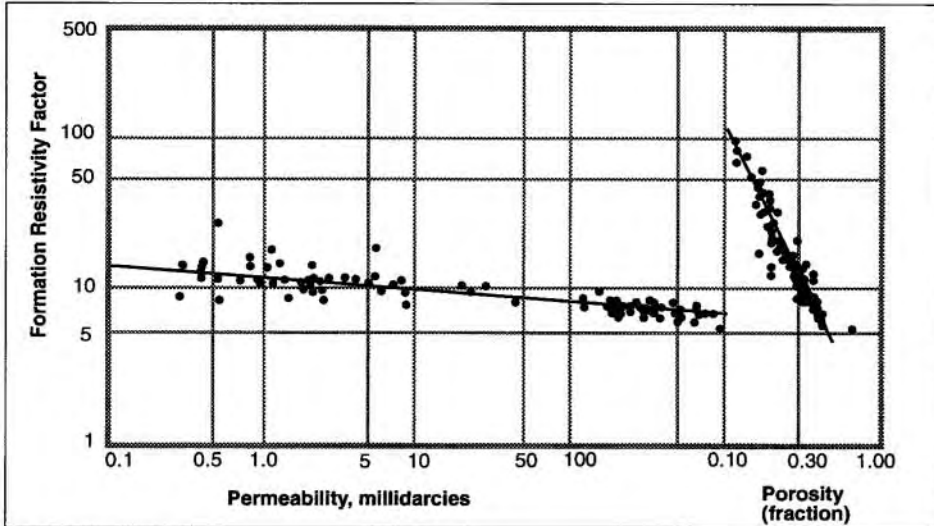


Figure 1.
 Porosity, permeability and Formation Factor data for the Nacatoch Formation.
 Permeabilities below 0.1 mD are not recorded.
 (From G. E. Archie (1943) Figure 2. with permission © SPE, 1943).

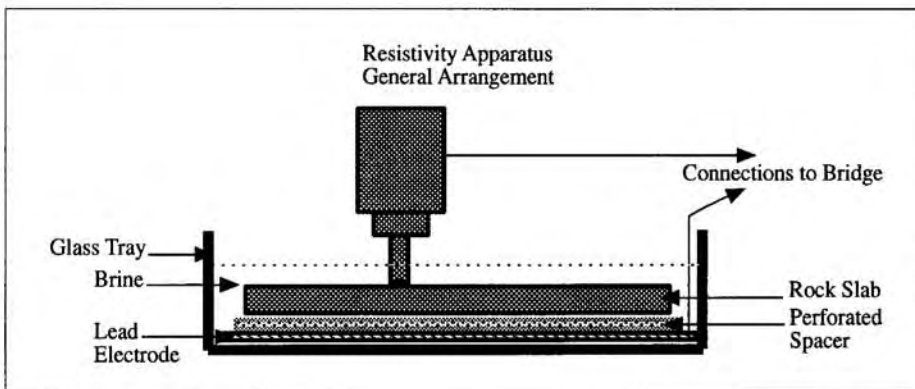


Figure 2.
 Schematic arrangement of the measuring system, showing the principal parts.

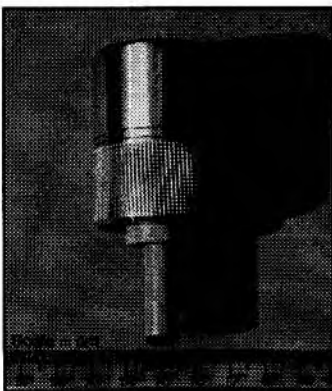


Figure 3.
 The Resistivity Probe used in this study.

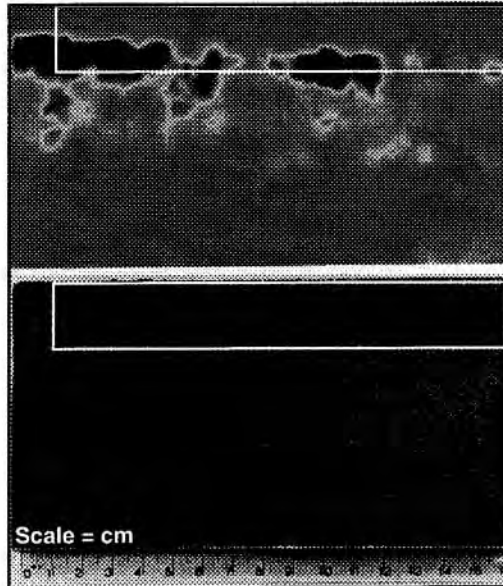


Figure 4.
The permeability map and the rock slab it was derived from. White rectangles outline the actual portion which was used in the acquisition of resistivity data

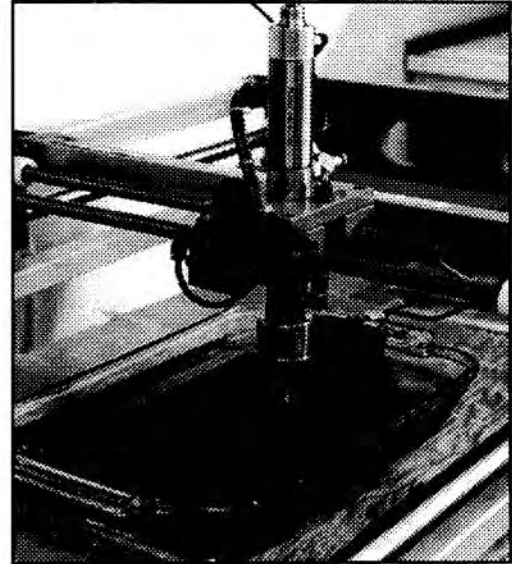


Figure 5.
The general arrangement of the resistivity apparatus and the sample.

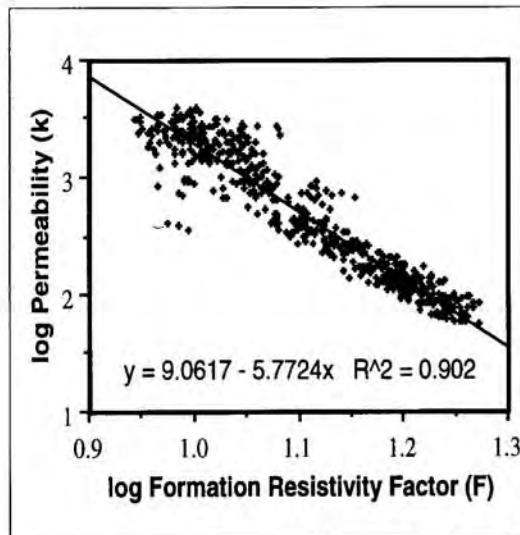


Figure 7.
Permeability - Formation resistivity factor relationship (lamina-scale) for the sample.

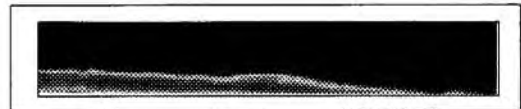


Figure 6.
The original resistivity image that was generated on the slab. The image was inverted to produce a better match with the permeability data.